Coordination Chemistry of Transition Metal Carbide Surfaces: Detailed Spectroscopic and Theoretical Investigations of CO Adsorption on TiC and VC (100) Surfaces

Stephen V. Didziulis* and Peter Frantz

Materials Science Department, Space Materials Laboratory, The Aerospace Corporation, El Segundo, California 90245

Luis C. Fernandez-Torres, Rebecca L. Guenard, Oussama El-bjeirami, and Scott S. Perry*

Department of Chemistry, University of Houston, Houston, Texas 77204-5641

Received: September 13, 2000; In Final Form: March 26, 2001

Detailed spectroscopic studies of the interaction of carbon monoxide (CO) with the (100) surfaces of titanium carbide (TiC) and vanadium carbide (VC) have been performed for the first time and analyzed to provide insight into the nature of the surface chemical interactions. The carbide materials are technologically important in extreme applications due to their remarkably high hardness and melting points. This work was pursued to develop a fundamental understanding of the surface bonding and reaction properties to enhance the use of TiC and VC as tribological materials and to gain insight into their potential use as catalysts. VC and TiC are both rocksalt materials but differ fundamentally in their electronic structure as the additional electron present in a formula unit of VC presents a significantly different surface bonding environment. CO has been used as a probe molecule to determine the relative electron accepting and donating tendencies of the substrates. Temperature-programmed desorption (TPD) has demonstrated that CO has a significantly higher heat of desorption on VC compared to TiC. High-resolution energy loss spectroscopy (HREELS) was used to measure surface vibrational frequencies, and the C—O stretch of reversibly adsorbed C—O is 2060 cm^{-1} on VC, and 2120 cm^{-1} on TiC, indicative of greater π-back-bonding on the VC surface. This enhanced back-bonding interaction is also observed in core level X-ray photoelectron spectroscopy satellite structure, and in valence band perturbations observed with ultraviolet photoelectron spectroscopy. Detailed analyses of these data show that CO has a slightly stronger σ-donor interaction with VC, but the stronger VC—CO bond is due primarily to the π-interaction that is essentially absent on the TiC surface. Density functional theory (DFT) has also been applied to small MC clusters that qualitatively reproduce the observed experimental trends. DFT also provides compelling evidence of the impact of the electronic structure difference on the CO interaction, as occupied d-orbitals in VC participate in the back-bonding interaction, but these levels are unoccupied in TiC. The results are entirely consistent with a simplified molecular orbital description of the materials that results in the surface metal atoms of TiC behaving like d^0 species and those of VC as d^1 species. These formal occupations are greatly tempered by covalent mixing with carbon atoms in the lattice, but the electronic structure clearly plays a dominant role in the surface bonding of the carbides, controlling their reactivity with lubricants and reactants with which they come into contact.

Introduction

Transition metal carbides possess numerous remarkable properties including high hardness and high melting points, making them desirable materials for extreme applications. For example, their use as antiwear coatings on tools and precision mechanical components is well documented.[1] A growing awareness of the unique surface chemical properties of these materials is developing, although relatively few fundamental surface chemistry studies of single-crystal materials have been published.[2] These surface properties will dictate the performance of lubricants and boundary additives in mechanical contacts involving these materials and will provide insight into the potential use of the carbides as catalysts.[3] In this paper, we present the first detailed spectroscopic studies of the interaction of carbon monoxide on the (100) surfaces of titanium carbide (TiC) and vanadium carbide (VC). The (100) surface of these rocksalt materials is nonpolar, with equal numbers of the metal and carbon atoms arrayed in a square lattice. The experimental techniques used to study the chemical bonding and reactivity of CO on these surfaces include temperature-programmed desorption (TPD), high-resolution electron energy loss spectroscopy (HREELS), X-ray photoelectron spectroscopy (XPS) and ultraviolet photoelectron spectroscopy (UPS). In addition, density functional theory (DFT) calculations have been performed on metal carbide clusters to provide greater insight into these bonding interactions.

The chemisorption of CO on metal and metal oxide surfaces has been studied extensively. The value of CO as a probe of surface bonding properties is well established and will be exploited in this work.[4] The strength of the surface bond with CO and the tendency for the molecule to decompose are strongly dependent on the extent to which the surfaces can π-bond with the molecule.[5] A substrate's ability to back-bond is governed by its electronic structure as electron density must be available in orbitals of appropriate symmetry and energy for this inter-

10.1021/jp003249b CCC: $20.00
Published on Web 05/10/2001

action to occur. The π-bonding interaction is usually reflected in the C—O stretching frequency, as partial occupation of the $2\pi^*$ orbital weakens the C—O bond. For example, on many transition metal surfaces, C—O stretching frequencies in the range of 2000 to 2100 cm^{-1} (significantly reduced from the gas-phase value of 2143 cm^{-1}) are quite common as the result of π-bonding with occupied metal d-levels.[6] Conversely, the occupied 3d-levels of ZnO are too deep in energy (pseudo core levels) to participate in a back-bonding interaction with CO.[7] Therefore, the molecule bonds only via a σ-donor interaction with the Zn sites, and the stretching frequency of this weakly adsorbed CO molecule actually increases above the gas-phase value.[8] Adsorption site geometry also plays a significant role in CO bonding, as the interaction with multiple atoms has been observed on metal surfaces, impacting spectroscopic results along with CO adsorption energies and surface reactivity.[5]

The electronic structure of transition metal carbides of the MC-type studied in this work has been described in a variety of publications and extensively reviewed by Johansson.[9] The materials crystallize in the rocksalt structure and have historically been termed as interstitial compounds to explain the octahedral bonding environment of the C atoms. Experimental investigations of the electronic structure have clearly shown that strong metal—carbon covalent bonding exists, resulting in the increased hardness and melting points.[10] In addition, the materials maintain fairly close proximity of nearest neighbor metal atoms in the lattice, potentially resulting in some metal—metal bonds.[11] Finally, some charge transfer from the metal to the carbon is also apparent from XPS core level studies, indicating the presence of ionic interactions, making the carbide label an appropriate one. The challenge in describing the surface electronic structure and its affect on chemisorption, therefore, lies in understanding the interplay among these forces and their potential influence on surface chemistry.

In recent publications, we have adopted a rather straightforward approach to describing the electronic structure of TiC and VC, and we have used this model to understand the adsorption and reaction of oxygen[12] and water[13] on these materials. As originally developed by Fischer,[14] the molecular orbital (MO) model treats the compounds as metal—carbon transition metal complexes (MC_6),$^{20-}$ producing the familiar diagram for a complex with O_h symmetry, as shown in Figure 1. Such an approach has been successfully employed for metal oxides and ionic materials with constituents much closer to their formal oxidation states than the carbides. Although the carbides are clearly extended lattices with delocalized electronic states and metallic-like conductivity, this MO model provides a useful description of local bonding interactions that explains many of our experimental results. In comparing VC and TiC electronic structures, the most important difference is the presence of an additional valence electron per formula unit of VC. Under O_h symmetry, this electron resides in a t_{2g} orbital that is predominantly V 3d in nature, and has been hypothesized to influence the surface chemisorption and reaction of VC in previous publications. When the symmetry is further reduced to reflect the ideal C_{4v} geometry of a (100) surface site, the d-manifold splits as shown in Figure 1, and one can use ligand field arguments to justify the lowest lying d-levels as being the e-symmetry $d_{xz,yz}$ levels that are the exact geometry required for back-bonding with CO.

The use of CO as a probe molecule is therefore ideal to determine the true utility of the MO model as will be shown in this paper. This work provides insights into the surface bonding and activation of small molecules on carbide surfaces and lays

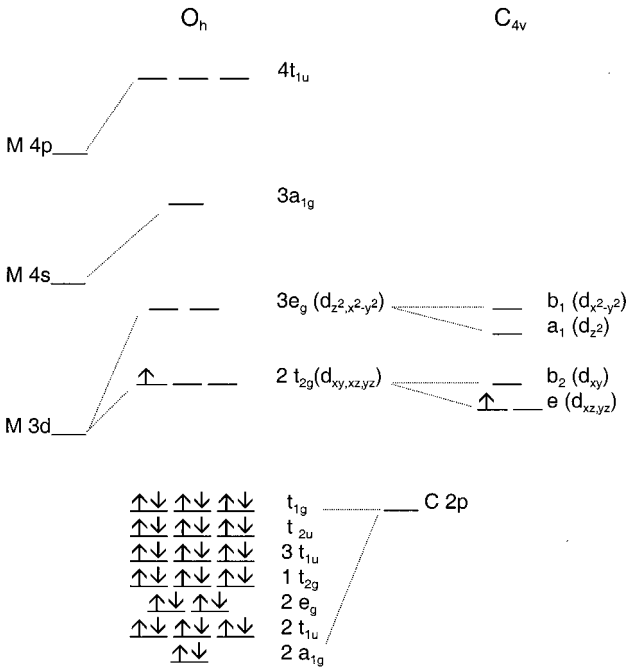

Figure 1. Molecular orbital diagram for a hypothetical $(VC_6)^{20-}$ complex, after Fischer (ref 13). Also included to the right is the d-manifold splitting expected for a C_{4v} metal site on the (100) surface, essentially a $(VC_5)^{16-}$ complex. When similar diagrams are generated for TiC, there is one less electron in the complexes and hence a formally unoccupied d-manifold.

the groundwork for understanding the surface chemistry of larger molecules of relevance in tribological work. TPD is used to probe the strength of the surface-CO bond, whereas the spectroscopic techniques probe adsorption site geometries, the electronic contributions to bonding, and detect surface reaction products. DFT calculations have been used to model the strength of the CO adsorption and to follow changes in the system energy levels to compare with the experimental results.

Experimental Section

This paper describes experiments performed at both The Aerospace Corporation and the University of Houston. Experiments were performed with (100) oriented single crystals of TiC and VC. Although the experiments were not performed on identical samples, the crystals were cut and prepared from the same boule using identical procedures. Independent XPS measurements performed at the two locations have verified similar surface stoichiometries and cleanliness of the samples following in-situ cleaning procedures.

The TiC (100) sample was obtained as a gift from UBE Industries of Japan. The growth techniques used to produce this sample have been described in the literature.[15] The crystal growers estimated the bulk stoichiometry to be $TiC_{0.9-0.92}$, although our XPS results indicate that the surface has a 1:1 stoichiometry (within the error of the technique). The VC (100) sample was obtained from the Linfield Research Institute, Linfield College, McMinnville, OR, and possessed a similar 1:1 surface stoichiometry, as measured by XPS. Both crystals were aligned by X-ray diffraction, then cut to within 1° of the desired crystallographic plane. They were polished with diamond paste down to a grit size of 0.25 μm and cleaned by rinsing with ethanol and acetone. Sample cleaning in ultrahigh vacuum entailed argon ion sputter/anneal cycles until the oxygen XPS signal was minimized. The accelerating potential of the Ar ion beam was 1000 V, and the samples were bombarded while

hot (870 K). This treatment was followed by electron beam heating (to 1473 K for TiC, 1273 K for VC) for 60−300 s with a resistively heated tungsten filament mounted directly behind the sample stage on the manipulator. Cooling to ∼150 K in the HREELS system was provided through a copper braid attached to a liquid nitrogen cooled heat sink. In the TPD system, the samples were mounted directly on a liquid nitrogen filled annular dewar, and thus allowed cooling to temperatures approximately 50 degrees colder than possible in the HREELS system. In both systems, the temperature was monitored with a type K thermocouple.

High-resolution electron energy loss spectra (HREELS) were collected at The Aerospace Corporation with a double-pass spectrometer (LK 2000, LK Technologies, Inc.) with a current measured at the sample of 10^{-10} A, a resolution defined by the elastic peak fwhm of 11 meV, and a typical elastic peak intensity of 3×10^5 counts/s. The spectra were obtained with incident beam energies of 7 eV; they were collected digitally and typically took 1 h each. The pass energy of the analyzer was 2 eV. The angle of incidence of the electrons was fixed at 60° with respect to the surface normal, and the signal was collected along the specular reflection.

Gas exposures (CO) in the HREELS experiments were performed by placing the sample in the path of a gas dosing system which consisted of a turbo-pumped gas supply, a leak valve, and a 9.75" dosing tube terminated by a channel plate. This system provided an enhancement in the mass adsorbed of approximately 25 times the mass deposited through back-filling the chamber. CO gas (99.99%, Matheson Gas Co.) was obtained from a cylinder and used without further purification.

TPD measurements were performed at the University of Houston in a UHV chamber with a base pressure of $<3 \times 10^{-10}$ Torr. The adsorption of CO (Matheson, 99.99%) was limited to the crystal faces through use of a pinhole doser.[16,17,18] This doser consisted of a 2 μm pinhole and a drift tube (5 mm ID) attached to a bellows. In vacuum, the sample face was positioned within 0.5 mm of the end of the tube, such that all gas effusing from the tube encountered the sample face. A fixed diffusion rate through the pinhole was achieved by holding a constant pressure on the gas handling side, providing excellent reproducibility of coverage. After dosing, the sample was positioned approximately 2 cm from the ionizer of a quadrupole mass spectrometer (Hiden Analytical, HAL IV). A linear heating rate was applied (4 K/s), and the following mass-to-charge ratios (m/q) were monitored: 28(CO^+), 12(C^+), 16(O^+). All data were collected using the same mass spectral sensitivities.

Photoelectron spectra (XPS and UPS) were collected at the University of Houston in the same vacuum system that houses the TPD setup. XPS experiments were carried out with an Omicron EA 125 energy analyzer and a VG dual anode source that provided Mg Kα radiation (1253.6 eV). Core level spectra were collected from a 1.5 mm spot on the sample surface with a 25 eV pass energy. Spectra were recorded with the energy analyzer situated 30° from surface normal. UPS measurements were performed using an UV lamp (Vacuum Generators). Helium (Matheson) was purified through a liquid nitrogen cooled molecular sieve before being introduced into the UV lamp to produce HeII (40.8 eV) and HeI (21.2 eV) radiation. Only He II data are presented in this paper. Spectra were collected along the surface normal with an Omicron EA 125 energy analyzer. DAT-125 Software (Spectra) was used to control and acquire the UPS spectra. Pass energy values of 15−20 eV were used in order to produce good data resolution. The sample was grounded to avoid charging effects. All binding energies are references to the Fermi level.

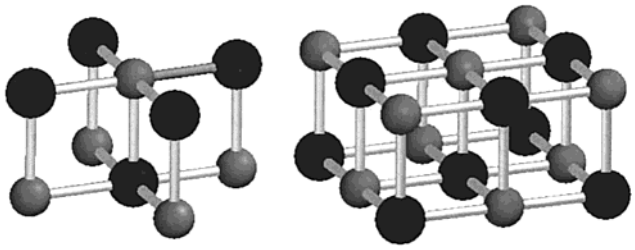

Figure 2. M_5C_5 and M_9C_9 clusters used in the DFT calculations to model the (100) surfaces of TiC and VC.

Density Functional Calculations. DFT calculations were performed using Titan version 1.0.1 software from Wavefunction, Inc., Irvine, CA. This program uses the computational program Jaguar 3.5 (Schrodinger, Inc., Portland, OR 1998) through a graphical user interface developed by Wavefunction. DFT calculations were performed using the B3LYP Model and the LACVP** pseudopotential basis set. Calculations were performed on the free CO molecule, M_5C_5, and M_9C_9 carbide clusters. The equilibrium geometry of the free CO molecule was calculated by the program and this energy was used for the comparisons cited below. The C−O bond length predicted by the calculation was 1.138 Å. The metal clusters shown in Figure 2 both have C_{4v} symmetry. No surface reconstructions were considered, the M−C−M cluster bond angles were rigorously constrained to be 90° and 180° in all cases, and the M−C bond distances were constrained to those of the respective lattice, 2.16 Å for TiC and 2.08 Å for VC. All calculations used convergence limits of 5.0×10^{-6} Hartree (H) for the SCF energy convergence criterion and 1.0×10^{-5} H for the SCF density convergence criterion.

To investigate the interaction of CO with the MC clusters, CO was bonded to both the high-symmetry C_{4v} metal and carbon atoms (see Figure 2) to create a fully coordinated surface species. For the M−CO interaction, the metal−CO bond length was varied over an approximate range of 1.90 to 2.30 Å in the M_9C_9 clusters to determine the optimum bond length, whereas the molecule was constrained to be normal to the surface, maintaining the C_{4v} symmetry. The C−O bond length was maintained at 1.15 Å for all calculations, allowing for some bond weakening as a result of adsorption. To determine the energy of interaction between the cluster and CO, the energies of the free CO and metal cluster were subtracted from the total energy of the CO bound complex. Although this process involves taking differences of large numbers, the convergence limits of the calculations were much more stringent than the differences in energies determined. In no instance did these calculations produce metal−CO bond energies that were unrealistic or that varied in a nonsystematic way. For the sake of comparison, a few calculations were performed with the CO molecule bound to the C_{4v} carbon atom. In these calculations, the C−CO bond length was always 1.53 Å and the normal geometry was maintained. No attempts were made to optimize this geometry.

Results

Temperature-Programmed Desorption. The results from the TPD studies are presented in Figure 3. In this figure, the molecular m/q 28 peak is monitored after adsorption of increasing amounts of CO on each surface at 100 K and subsequent temperature ramping. In Figure 3a, a single desorption feature is evident on TiC with a desorption maximum at 145 K at the lowest exposure studied, and decreasing to 139 K

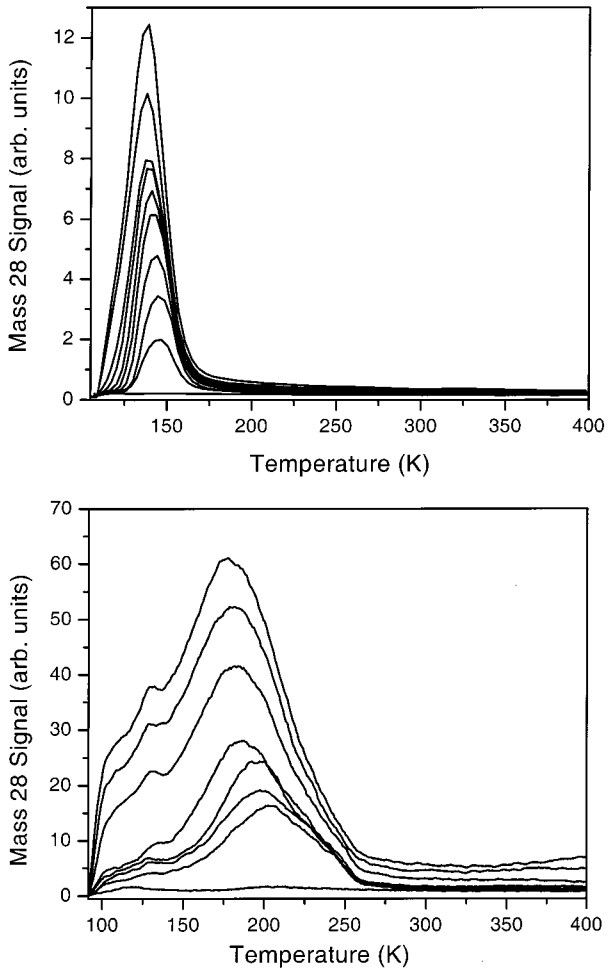

Figure 3. $m/q = 28$ TPD results obtained after adsorption of increasing amounts of CO at 100 K on (a) TiC (100) and (b) VC (100).

with increasing coverage. At the highest exposures, the desorption peak broadens slightly to lower temperature but no indication of surface saturation is evident. The TPD results from the VC surface in Figure 3b are more complex. At low exposures, a broad peak with a desorption maximum at approximately 200 K is evident, along with a prominent shoulder at 240 K. In other experiments using lower exposures, a feature was observed at 250 K that shifted to 200 K with increasing exposure. With increasing coverage, the main desorption feature continues to shift to lower temperature, eventually reaching 170 K. An additional peak becomes more apparent with increasing exposure, with a constant desorption temperature of 130 K. The significantly higher desorption temperature for the majority of CO adsorbed on VC shows that VC forms stronger reversible bonds with CO than does TiC. The relative strengths of these interactions were further probed through variable heating rate TPD to determine the enthalpy of desorption of CO for these surface species, which is equal to the heat of adsorption for nonactivated processes.

The results of the variable heating rate experiments for TiC are presented in Figure 4, which plots $\ln(\beta/T_d^2)$ vs $1/T_d$, where β is the heating rate and T_d is the temperature of the desorption maximum for a given heating ramp.[19] The resulting Arrhenius plot gives a straight line, and the slope is equal to $-\Delta H_{des}/R$, where ΔH_{des} is desorption enthalpy, and R is the ideal gas constant. For this experiment, the slope was -5800 K, which produces a ΔH_{des} of 11.5 ± 2 kcal/mol. Repeated attempts to generate similar results on VC (100) have resulted in unrealistically low values for ΔH_{des}, ranging from 6 to 8 kcal/mol. One possible explanation for this is a significantly different preexponential factor arising due to increased repulsion among the adsorbed CO species on VC. From the difference in the desorption maximum temperatures measured in the TPD, one can estimate that the ΔH_{des} for the VC surface should be approximately 16 to 19 kcal/mol at low coverage. It is apparent that CO reversibly binds to both of the surfaces in a fairly weak fashion, but it is also clear that the interaction on VC is significantly stronger, and surface spectroscopies have been used to probe the origins of this stronger bond.

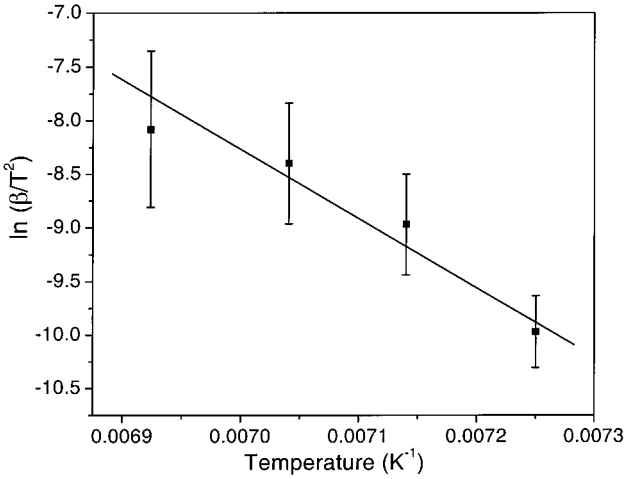

Figure 4. Arrhenius plot of $\ln(\beta/T_d^2)$ vs $1/T_d$ used to determine the heat of desorption for CO from the TiC (100) data using variable heat ramp TPD. The slope of the linear fit to the points is -5800, which is multiplied by the gas constant ($R = 1.987$ cal/molK) to provide the heat of desorption.

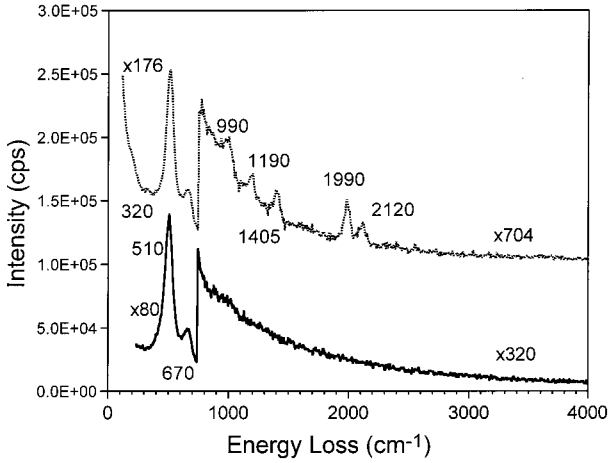

Figure 5. HREELS data obtained on clean and CO exposed TiC (100) surface. Data obtained at 150 K are shown for the clean TiC (100) surface and in a 1×10^{-8} Torr of CO ambient. The positions of the loss features attributed to the substrate and CO are included on the figure. In these and all HREELS data that follow, the spectra have been normalized to the intensity of the elastic peak. The factors by which the data were multiplied for normalization are listed on each spectrum.

High-Resolution Electron Energy Loss Spectroscopy. Figure 5 presents HREELS results from CO adsorption studies on the TiC (100) surface. Experimental limitations of the HREELS system manipulator only allowed study at temperatures of 150 K and above on these chemical systems. The clean surface HREELS data (lower spectrum) reveals one major loss feature at 510 cm^{-1} attributed to the Ti—C stretching frequency and a smaller peak at 670 cm^{-1} attributed to a Ti—O—Ti species

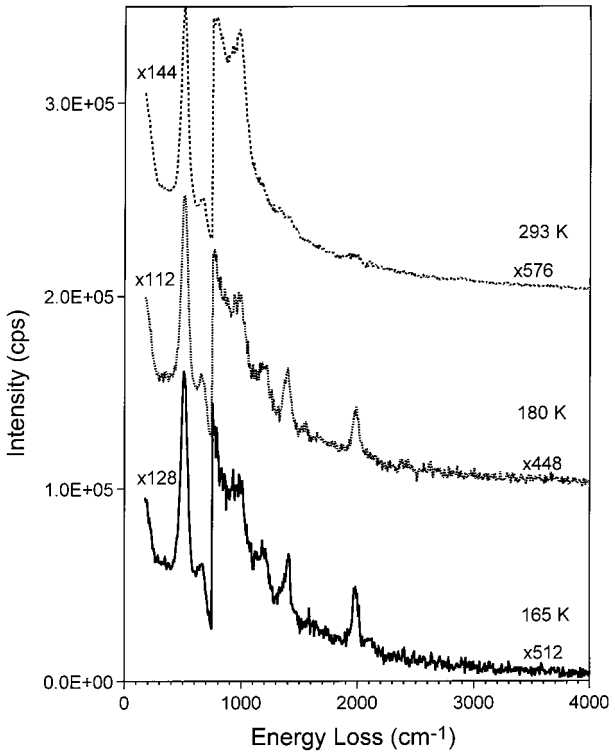

Figure 6. HREELS data obtained from the CO/TiC (100) surface after removal of the CO ambient and warming to 165, 180, and 293 K, before cooling back to 150 K to collect the data.

arising from the presence of a persistent oxygen impurity that could not be removed by our cleaning process. Initial CO exposures (up to 25 L — not shown) on the TiC surface at 150 K did not reveal spectroscopic changes that could be definitively linked to reversible CO adsorption or decomposition. This is not surprising because the adsorption temperature in the HREELS system is contained within the desorption feature of the TPD data presented in Figure 3a. The absence of CO features in the HREELS spectrum following a 25 L exposure at 150 K confirms the weak chemical interaction of CO with the majority surface sites present on TiC.

To probe the TiC—CO surface complex at 150 K, we obtained HREELS data with a 1×10^{-8} Torr ambient of CO in the analysis chamber. The results of this experiment are presented in Figure 5 (upper spectrum). Several weak peaks are observed in this spectrum. Peaks observed at 2120 and 1990 cm^{-1} are assigned as C—O stretches from two distinct surface species. In addition, a weak peak at 320 cm^{-1} is attributed to a Ti—CO stretch. Other spectral features are also present, including loss peaks at 990, 1190, and 1405 cm^{-1}. These peaks are not produced by molecular CO adsorption on single atom atop sites. The 990 cm^{-1} peak is quite similar to weak features observed after oxygen adsorption on TiC and has been ascribed to a surface Ti═O species. Low-frequency C—O stretches have been observed on some metal surfaces,[20,21] but we will delay further discussion of the possible assignments of the other spectral features to the discussion section below.

To gain a greater understanding of the HREELS results, data were taken after removing the CO ambient, warming to selected temperatures and recooling to 150 K to collect data. After pumpout of the CO ambient at 150 K (data not shown), the weak loss peaks at 2120 and 320 cm^{-1} become weaker, confirming that these features arise from a reversibly adsorbed CO species. Data obtained after heating to 165 K (Figure 6) show a very weak peak at 2120 cm^{-1}, whereas the other loss

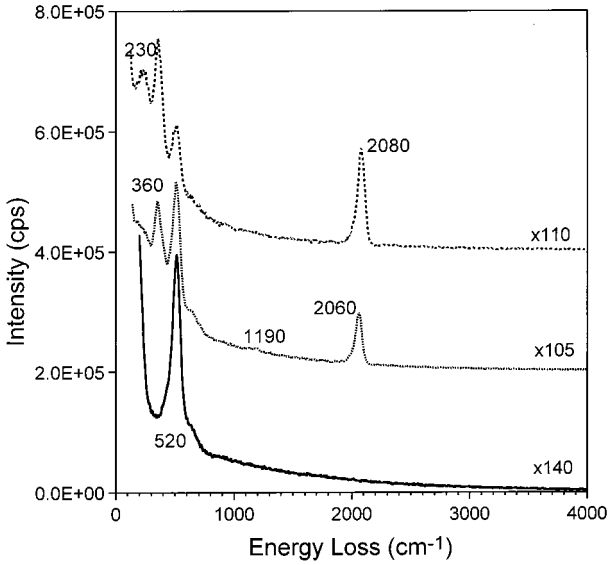

Figure 7. HREELS data obtained on clean (bottom) and CO exposed VC (100) at 150 K. The CO data were obtained after a 25 L exposure (middle) and in a 1×10^{-8} Torr ambient (top). The substrate and CO-related features are labeled on the figure.

features retain their intensity. After the sample is warmed to 180 K, there is no trace of the 2120 cm^{-1} feature, and further warming to room temperature leads to a loss of intensity of the peaks at 1990, 1405, and 1190 cm^{-1} whereas the peak at 990 cm^{-1} gains intensity. These results show that a small amount of CO strongly adsorbs to the TiC (100), and undergoes chemical changes eventually leading to a surface Ti═O species.

In contrast to the TiC data, HREELS data obtained from VC (100) at 150 K show very large loss features attributable to adsorbed CO. In Figure 7, the clean HREELS spectrum of VC is shown along with data obtained after a 25 L CO exposure and a spectrum obtained in a 1×10^{-8} Torr of CO ambient. In the clean spectrum, only a single loss feature is present at 520 cm^{-1}, attributed to the V—C stretch. There is a slight broadening of this peak to higher energy, but clearly, no well-resolved second peak is observed as on TiC, consistent with our ability to clean VC more completely. Upon exposure to 25 L of CO, very strong loss features are observed at 2060 and 360 cm^{-1}, corresponding to the C—O and V—CO stretches of a chemisorbed surface species. In addition, a weak peak is observed near 1190 cm^{-1}, similar to one of the features seen on TiC. In the data obtained in the CO ambient, the intensity of the C—O stretch has increased, and the peak shifts to higher energy, now centered around 2080 cm^{-1}. The 360 cm^{-1} peak has also increased in intensity, and a new feature centered at 230 cm^{-1} has appeared. No other loss features are observed in the ambient data.

Figure 8 presents HREELS data taken after warming the CO exposed VC surface to increasingly higher temperatures. The 1×10^{-8} Torr of CO ambient data are shown at the bottom of the figure. After the CO ambient has been pumped out and the sample warmed to 165 K, the C—O stretch loses intensity and shifts back to 2060 cm^{-1}, and both of the low energy loss features lose intensity, in particular the feature at 230 cm^{-1}. Additional peaks are now observed in the region between 600 and 1500 cm^{-1}, and these will be detailed below. After the sample has been warmed to 180 K, the C—O stretch and the V—CO stretch both lose more intensity. Further reductions are observed after warming to 200 K, but some signal intensity persists. At room temperature, the features attributed to the CO molecule chemisorbed to a single surface atom are absent, and

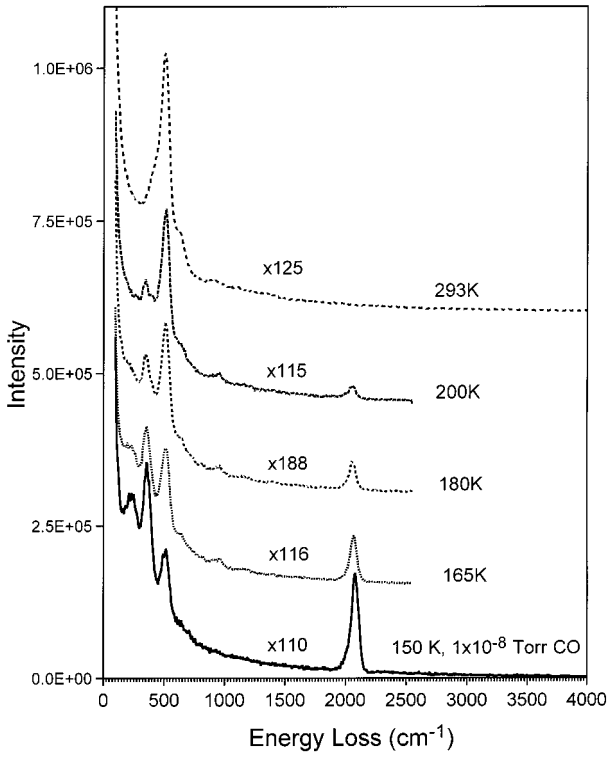

Figure 8. HREELS data obtained on the CO exposed VC surface following pumpout of the CO ambient and warming to the temperatures indicated. All data were collected after cooling back to approximately 150K.

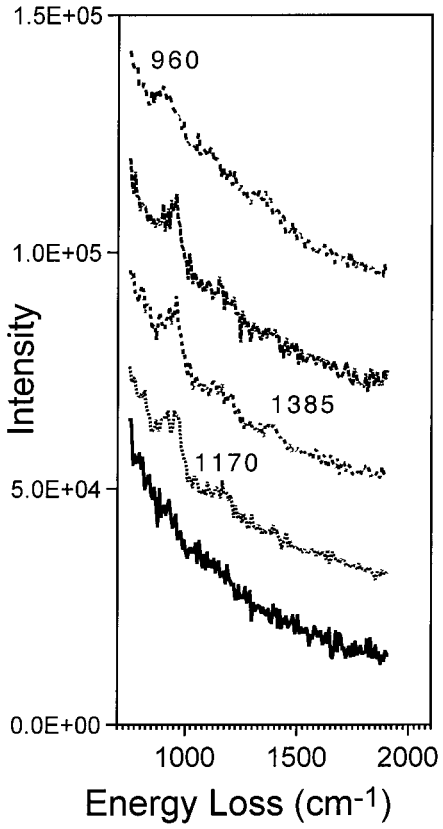

Figure 9. HREELS data in the region of 700−1900 cm^{-1} from the data presented in Figure 8 on the CO/VC surface.

the TPD data certainly indicate that the surface species leading to the molecular desorption of CO should now have been desorbed.

The regions between 700 and 1900 cm^{-1} in the VC data from Figure 8 are magnified in Figure 9. These data show the clear presence of peaks near 960, 1170, and 1385 cm^{-1}. The locations of these peaks are quite similar to features observed in the TiC data discussed above, and probably arise from similar surface species. Unlike the TiC data, the peaks at 1170 and 1385 cm^{-1} are always weaker than the 960 cm^{-1} feature, which is almost certainly the V═O surface vanadyl. In addition, the shoulder on the high energy side of the V−C stretch in Figure 8 appears to be more prominent in the CO exposed data as compared to the clean surface, suggesting the formation of some of the V−O−V surface species.

The HREELS data for the TiC and VC (100) surfaces are entirely consistent with the TPD results. The data show that more molecular CO is chemisorbed to VC under the HREELS conditions studied, indicating that CO has a stronger surface bond with VC than with TiC. The lower C−O stretching frequency observed for the reversibly bound molecules on VC (2060 cm^{-1} for VC, 2120 cm^{-1} for TiC) is indicative of greater π-back-bonding on VC. Both surfaces also appear to irreversibly bind and react with a small fraction of the adsorbed CO.

X-ray Photoelectron Spectroscopy. The C 1s and O 1s XPS core levels from clean and CO exposed TiC and VC are presented in Figures 10 and 11 after the substrate background signal has been subtracted from the data. On the clean surfaces, the carbide C 1s peak appears at binding energies of 281.4 for TiC and 282.7 for VC. Each clean surface also has a small O signal, located at 530.7−531 eV, consistent with a metal oxide impurity. After exposure to CO at a temperature of 120K, each surface displays new spectral features that can be ascribed to the adsorption of CO.

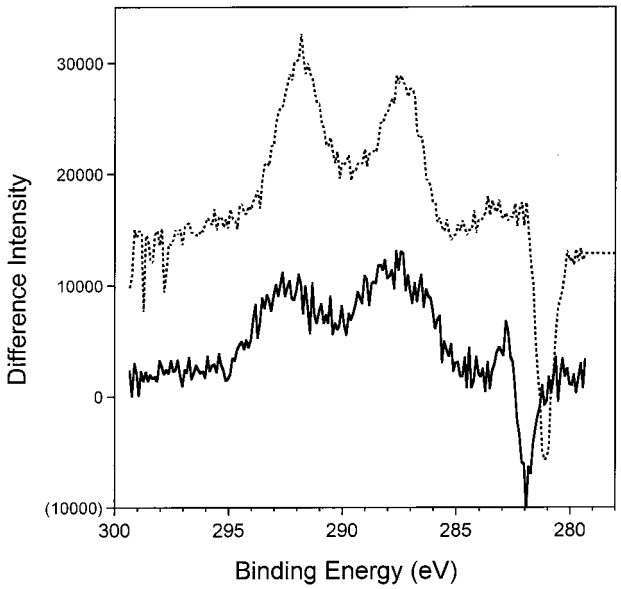

Figure 10. XPS difference spectra of the C 1s region of TiC (top) and VC (bottom) (100) surfaces exposed to monolayer forming levels of CO at 120 K. The spectra of the clean surfaces were scaled to the intensity of the substrate C 1s peak and subtracted from the CO exposed data. The negative peak evident in both spectra is the result of small differences in the peak shape of the substrate signal after CO adsorption.

The C 1s region from TiC after CO adsorption shows two new spectral features. The peaks are located at binding energies of 287.4 and 291.8 eV. As shown in Figure 10 (top), subtraction of the clean TiC spectrum from the CO data reveals that the peaks are of nearly equal intensity, and the integrated intensity obtained from a data fit indicates that the deeper binding energy peak is more intense by a factor of 1.2. All data fits were

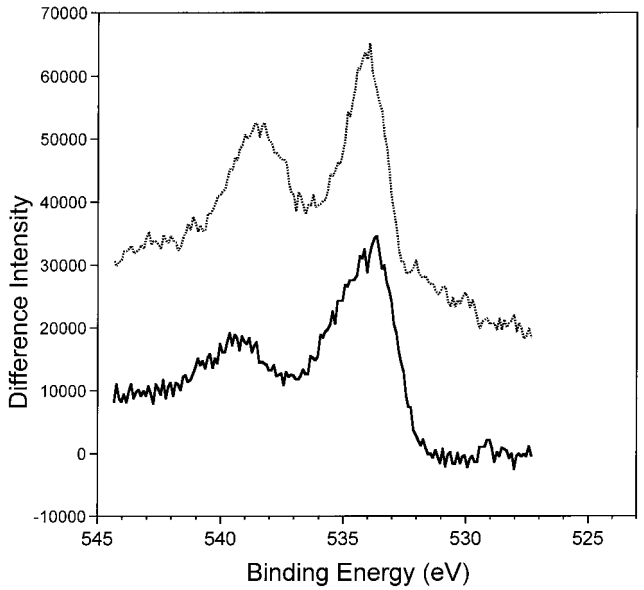

Figure 11. XPS difference spectra of the O 1s region of TiC (top) and VC (bottom) surfaces exposed to monolayer forming amounts of CO at 120 K. These data were obtained in the same experiment as those presented in Figure 10. Once again, the clean surface spectrum was subtracted from the CO exposed data to remove contributions from surface oxygen impurities.

TABLE 1: XPS Core Level Peak Binding Energies and Relative Intensities for CO Adsorbed on TiC and VC (100)

peak	main BE (eV)	satellite BE (eV)	delta (eV)	I_{sat}/I_{main}
C 1s on TiC	287.4	291.8	4.4	1.24
O 1s on TiC	534.1	538.4	4.3	0.84
C 1s on VC	287.7	292.5	4.8	0.69
O 1s on VC	533.8	539.1	5.3	0.34

performed using Gaussian-broadened Lorentzian peaks and a Shirley background. Similarly, the O 1s region from TiC exposed to CO in Figure 11 (top) possesses two new peaks, with binding energies 534.1 and 538.4 eV. In these data, the lower binding energy feature is slightly more intense but the splitting is similar to the two peaks found in the C 1s data.

Figure 10 (bottom) presents the C 1s difference spectrum from VC exposed to saturation levels of CO at 120 K. As observed in the TiC data, two new peaks are present in the C 1s data, although they are not as obvious as on TiC in the raw data. The peaks are broader on VC, and are located at binding energies of 287.7 and 292.5 eV, with the lower binding energy feature more intense. The same trends are observed in the O 1s data shown in Figure 11 (bottom), where two peaks are clearly evident at energies of 533.8 and 539.1 eV. In these data, the lower binding energy feature is clearly more intense than the deeper energy peak. The data are summarized in Table 1, where the binding energies and the relative intensities of the lower binding energy main peak and the deeper binding energy satellite peak obtained from fits are provided.

The presence of multiple core level XPS peaks upon adsorption of CO has been noted previously.[22] The deeper binding energy satellite peak is observed when CO is chemisorbed to a surface with some π-back-bonding character. The intensity of the satellite peak increases as the adsorption strength decreases, which seems contradictory to the requirement for back-bonding.[23] The reasons for these observations will be addressed in the discussion section below.

Ultraviolet Photoelectron Spectroscopy. Figure 12 presents the valence band photoemission spectra of the clean TiC (100) (lower spectrum) and a surface saturated with CO at 120 K

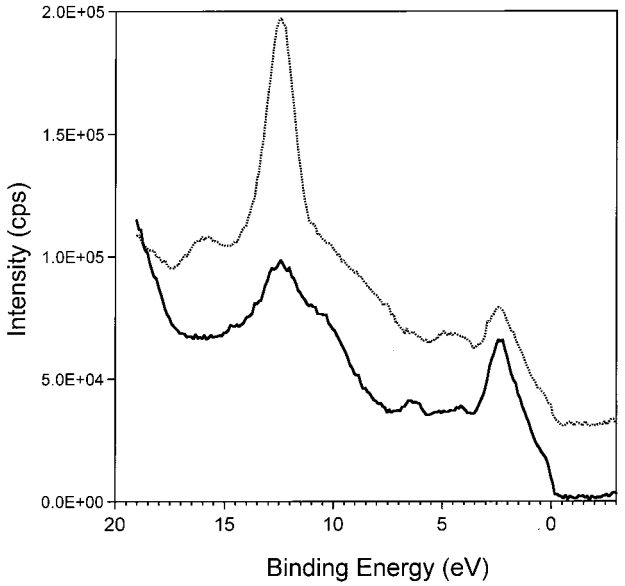

Figure 12. He II UPS data obtained from the clean (bottom) and CO exposed (top) TiC (100) surface.

obtained with HeII radiation. The clean spectrum is similar to those obtained previously for this surface at this photon energy.[10] The major peak near 2.3 eV is photoemission from predominantly C 2p based levels with significant mixing with Ti 3d character. Smaller peaks near 4.5 and 6.5 eV are also C 2p features that have been shifted to deeper binding energies through stronger covalent interactions. The C 2s peak appears near 10.5 eV. The large peak at approximately 12.5 eV is the Ti $M_{2,3}VV$ Auger peak that has been documented previously in synchrotron radiation studies.[10]

Upon adsorption of CO, several spectral changes are evident: a very large peak centered at 12.5 eV, a smaller peak near 16 eV, an increased background, and an apparent drop in the intensity of the main TiC peak at 2.3 eV. These changes are better observed in the two upper difference spectra presented in Figure 13. These spectra on TiC were obtained in two ways since absolute intensity changes in the substrate photoemission can be the result of many factors, including a variable photon flux, attenuation by adsorbed species, and the effects of adsorbate bonding on the surface electronic structure. The upper two difference spectra were obtained by normalizing to the background in the range of 4−6 eV (solid line) and by normalizing to the intensity of the main TiC feature at 2.3 eV (dotted line). Both difference spectra show three distinct peaks that can be attributed to CO adsorption—a small, broad feature centered at 8.2 eV, an intense peak at 12.5 eV, and a small peak at 15.9 eV. In the data normalized to the background, the main TiC feature has decreased in intensity.

The clean VC (100) spectrum (lower) in Figure 14 is different than the TiC data, reflecting the different electronic structure of the materials. Specifically, VC has an additional sharp feature centered at 0.4 eV relative to the Fermi level arising from photoemission of the occupied V 3d level. The other main peaks are the C 2p (3.3 eV) and C 2s (11.7 eV) photoemission, similar to those found in TiC, but shifted to deeper binding energy by approximately 1 eV. Upon adsorption of CO, two new peaks are observed at binding energies of 12.4 and 8.5 eV. Only these peaks are observed in the difference spectrum presented in Figure 13 (bottom), which also highlights the decrease in the intensity of the two main VC peaks as evidenced by dips in the difference data. The difference data were scaled to the background intensity. When scaled to the clean C 2p peak intensities

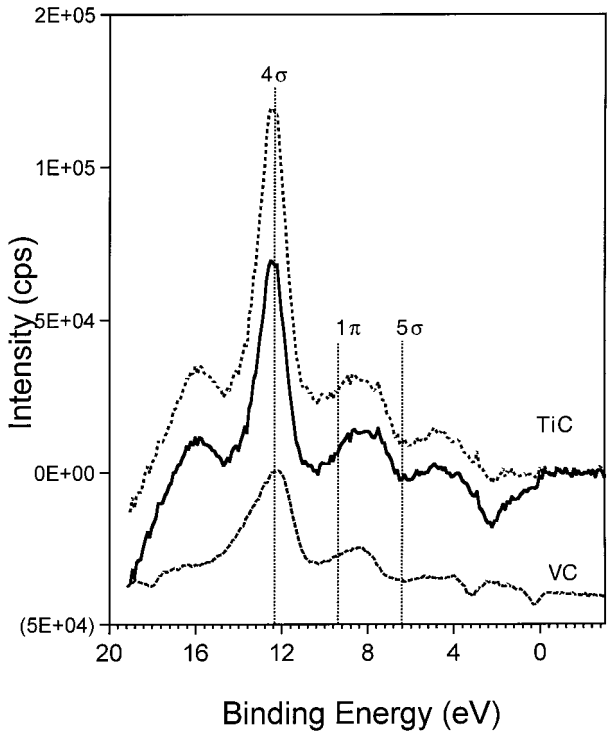

Figure 13. UPS difference spectra obtained by subtracting the clean TiC and VC spectra from the data obtained after CO exposure. The top two spectra are from the CO/TiC surface, with the background scaled in two different manners. The bottom spectrum is from the CO/VC surface. The dotted vertical lines show the positions of the gas-phase CO UPS peaks, referenced to the 4σ level.

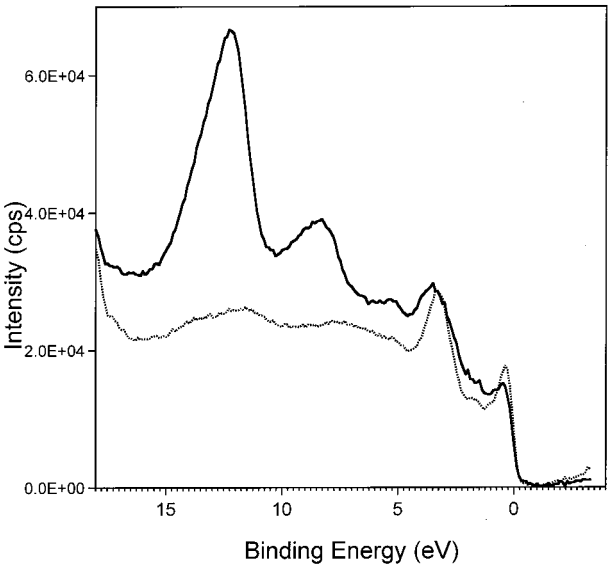

Figure 14. He II UPS data obtained from the clean and CO exposed (solid line) VC (100) surface.

as is done in Figure 14, the background is raised significantly, and the VC peaks appear to broaden to deeper binding energy. The intensity decrease of the V 3d peak is greater than the impact on the C 2p band, indicating a greater perturbation caused by the adsorbed molecule. The V peak maximum appears to shift to deeper binding energy by 0.1 eV. In addition, a shoulder appears at about 0.4 eV deeper energy than the original peak. Although this shoulder is barely observable above the noise, it is present in several spectra taken under a variety of conditions. In evaluating these changes, one must also be aware of the impact of the 48.4 eV He line on the spectrum. The very intense 12.3 eV peak would appear at 4.7 eV and, hence, overlap the C 2p band on its deeper binding energy side. In addition, the much weaker 8.5 eV peak in the He II spectrum would appear very close to the position of the V 3d shoulder discussed above. Without a monochromatic source it is very difficult to deconvolute these effects.

In the gas phase, the photoelectron spectrum of CO has three peaks, resulting from photoemission from the 5σ (ionization potential of 14.0 eV), 1π (16.9 eV) and 4σ (19.7 eV) molecular orbitals. The binding energy position of these peaks upon adsorption is substrate dependent, varying due to bonding and relaxation effects but their energy splitting is typically more sensitive to bonding effects. Specifically, electron donation to the surface from the 5σ orbital stabilizes the level such that it often overlaps with the 1π in UPS data.[24] In our data, this is most readily observed in the CO/VC spectrum, which shows two distinct peaks with binding energies of 12.4 and 8.5 eV, which we assign as the 4σ and 1π/5σ levels. In Figure 13, the positions of the gas-phase CO peaks are superimposed on our difference spectra, with the gas-phase data shifted such that the data are aligned to the 4σ peaks. The 3.9 eV splitting on VC is greater than the 4σ−1π gas-phase value, and this can be attributed in part to the presence of the 5σ at a lower binding energy than the 1π, yet still overlapping. Three peaks are evident in the CO/TiC data, and we assign the peak at 12.5 eV as the 4σ and the broad feature at 8.2 eV as the 1π/5σ combination. Both the greater splitting between these peaks and the breadth of the 1π/5σ level indicate that the 5σ does not overlap the 1π as strongly for CO chemisorbed to TiC, indicative of a weaker bonding interaction. The third peak in the CO/TiC spectrum is located at 15.9 eV, and this satellite peak is analogous to the satellite observed in the core level spectra discussed above and has been observed for other weakly adsorbed systems.[25] Differences in the UPS data of the two materials suggest differences in the surface bonds formed. To quantify these differences, detailed data analyses will be performed in the discussion section.

Electronic Structure Calculations. DFT calculations were performed on M_5C_5 and M_9C_9 clusters having the general structures shown in Figure 2. Such clusters provide the appropriate stoichiometry for the system and are the smallest, high symmetry (C_{4v}) clusters that possess at least one metal and one carbon atom with their complete (100) surface bonding environment. These calculations will be used for two purposes. First, the total energy of the clusters and CO will be compared with and without a chemisorption bond in an effort to determine the strength of the surface-CO bond. Second, the changes observed in the CO and substrate orbital energies upon adsorption will be reported to provide insight into the nature of the bonding interactions occurring in these systems. The adsorption of CO both to a metal and a carbon site was probed.

The Ti—CO bond distance was varied on the Ti_9C_9 clusters in the range of 2.10 to 2.25 Å (optimized at 2.20 Å, although the effect was < 0.01 eV in this range) to provide the most stable cluster while maintaining a fixed C—O bond distance. We recognize that the C—O bond length is very sensitive to the amount of back-bonding and the optimized bond length will be explored in future work. The energy difference between the unbound CO and the clusters and the CO-cluster are presented in Table 2. The result on the Ti_5C_5 cluster with a 2.20 Å Ti—CO bond length is also provided.

On the smaller cluster, the Ti—CO complex was more stable than the unbonded CO/cluster pair by −0.954 eV, which translates to a ΔH_{ads} of −22 kcal/mol. The value obtained on

TABLE 2: Energy Stabilization Predicted by DFT for CO Adsorbed on TiC and VC Clusters

adsorption site in cluster (bond length in Å)	energy stabilization (eV)
CO—Ti on Ti_5C_5 (2.20)	−0.954
CO—Ti onTi_9C_9 (2.20)	−0.549
CO—C on Ti_5C_5 (1.53)	−0.583
CO—C on Ti_9C_9 (1.53)	+2.52
CO—V on V_5C_5 (2.00)	−1.24
CO—V on V_9C_9 (2.00)	−1.07
CO—C on V_5C_5 (1.53)	+3.84
CO—C on V_9C_9 (1.53)	+1.83

TABLE 3: Positions of the CO Valence Levels (in eV) Calculated by DFT as Outlined in the Text

species	4σ	1π	5σ	$5\sigma-4\sigma$	$2\pi^*$	$2\pi^*-4\sigma$
free CO	−15.51	−12.72	−10.11	5.40	−0.59	14.92
CO—Ti_5C_5	−15.16	−12.27	−11.23	3.93	+0.33	15.49
CO—Ti_9C_9	−15.85	−12.77	−11.69	4.16	−0.40	15.45
CO—V_5C_5	−15.18	−12.27	−11.69	3.49	+0.33	15.51
CO—V_9C_9	−15.12	−12.18	−11.43	3.69	+0.33	15.45

the larger cluster was −12.7 kcal/mol, similar to the desorption energy obtained from the TPD experiments. Alternatively, for adsorption on a carbon site, we get conflicting results for the two TiC clusters. On the small cluster, we calculate a significant energy stabilization for CO adsorbed to a carbon atom, whereas on the larger cluster, this interaction is highly unfavorable (we did not try to optimize the C—CO bond distance). For each cluster, CO bonding with Ti is favored over bonding to the C, and the larger cluster indicates that the C—CO interaction is unlikely. As might be expected, the larger cluster appears to provide a more realistic result for CO adsorption energy.

The results for the VC clusters provide very strong evidence for stronger CO adsorption relative to TiC. For the smaller V_5C_5 cluster, we calculate a bonding energy of −28.6 kcal/mol for V—CO. Calculations for CO adsorbed on the V_9C_9 cluster produce an energy of −24.6 kcal/mol, a significantly stronger bond than that predicted for CO interacting with TiC. CO bonded to the carbon atom on both VC clusters is shown to be very unstable. The predicted adsorption energies for VC are somewhat higher than we believe the TPD peak temperatures indicate, approximately 18 kcal/mol. We do observe a trend of decreasing CO adsorption energy with increasing cluster size, and surmise that with even larger clusters, the adsorption energy would drop further. For example, the charge on the vanadium atom likely plays an important role in the relative surface donor and acceptor interactions. The charge on the central vanadium atom in the bare clusters, calculated from Mulliken populations, decreases from +1.53 to +1.13 as the cluster size increases from the V_5C_5 to V_9C_9. We expect that as more atoms in the cluster have their complete bonding environment, that this value could be further reduced, impacting the adsorption energy of CO. This work is currently being extended to calculations on larger clusters.

The energy level shifts calculated after CO adsorption provide insight into bonding and enable a comparison to our experimental results and interpretation. The calculation on the free CO molecule generates orbital positions provided in Table 3. The calculated 5.40 eV $4\sigma-5\sigma$ splitting is less than the experimental value of 5.7 eV obtained by photoemission, whereas the calculated $4\sigma-1\pi$ splitting of 2.79 eV is indistinguishable from the experimental value. These calculations also place the empty $2\pi^*$ level at 14.92 eV above the 4σ. In bonding to the cluster, we assume that the more stable interaction of CO with the metal surface atom will be the exclusive adsorption site, and we compare the positions of the CO orbitals from both cluster sizes in Table 3. The $4\sigma-5\sigma$ splitting is 4.16 eV for the Ti_9C_9 cluster, whereas the $4\sigma-2\pi^*$ splitting 15.45 eV. Compared to the values for free CO and assuming that the 4σ level is not perturbed by bonding interactions, the 5σ has been stabilized by the σ-bonding interaction with TiC by 1.24 eV on the larger cluster. The $2\pi^*$ has been destabilized by 0.53 eV by π-overlap.

The positions of the CO energy levels from the CO—V_5C_5 and CO—V_9C_9 clusters are included in Table 3. In the larger cluster, the 4σ-5σ splitting and the $4\sigma-2\pi^*$ splitting are 3.69 and 15.45 eV, respectively. As with the TiC results, we see that the cluster size has relatively little impact on the position of the $2\pi^*$ level, implying little impact on π-bonding interaction but a significant effect on the 5σ position. The calculations predict that σ-bonding interactions on VC have stabilized the 5σ level by 1.91 eV in the smaller cluster and 1.71 eV in the larger. These values are significantly larger than those calculated for the TiC interactions. The $2\pi^*$ level has been destabilized by 0.53 eV, a result that is virtually identical to the TiC calculations.

The substrate wave functions for the clusters are quite complex and delocalized, making a definitive assignment of specific atomic contributions to surface levels challenging. We will discuss these results in more detail in a subsequent publication. However, we can pinpoint the level having significant metal $3d_{xz,yz}$ character on the atom bonding with the CO molecule on both M_9C_9 clusters. With CO bonded, the Ti $3d_{xz,yz}$ level is located at −2.50 eV, which has shifted from −2.28 eV in the Ti_9C_9 cluster without CO. However, the highest occupied molecular orbital (HOMO) for the TiC clusters is at −4.54 eV for the CO bound cluster and −4.50 eV for the bare cluster. So, even though the $d_{xz,yx}$ levels are stabilized by 0.2 eV through the π-overlap, they are unoccupied and do not contribute to CO bonding. Alternatively, the V $3d_{xz,yz}$ level for the CO—V_9C_9 complex shifts from −4.07 to −4.21 eV after CO bonding. Although this shift is small, there are several other orbitals having $d_{xz,yz}$ contributions that are also impacted in the calculation. Importantly, the HOMO in the CO-bound V_9C_9 cluster is at −3.56 eV. This clearly indicates that the $d_{xz,yz}$ orbital is occupied and contributes to the V—CO interaction. The findings are consistent with the simplified MO model that has been used as a starting point in understanding the bonding and surface chemistry of these materials.

Discussion

CO Adsorption. The TPD data provide clear evidence that CO has a stronger reversible bonding interaction with the VC (100) surface than with TiC (100), approximately 18 kcal/mol vs 12 kcal/mol. In this section, we will provide spectroscopic analyses and discussions that lead to the conclusion that this stronger surface bond is due primarily to π-back-bonding interactions on VC that are much weaker on TiC. Before that work is presented, we note that the 12 kcal/mol desorption enthalpy for TiC is very similar to the adsorption enthalpy measured for CO on the zinc sites of ZnO.[26] It has been shown experimentally and theoretically that no back-bonding exists for the CO—ZnO interaction, and the similar adsorption energy on TiC suggests that σ-donor interactions dominate CO adsorption on TiC. The interaction with TiO_2 surfaces has also been studied, and it appears that CO will only chemisorb at oxygen vacancy defect sites.[27] In related work, TPD studies of CO desorption on oxidized polycrystalline titanium foil surfaces in which the Ti oxidation state was systematically altered provided a desorption energy of 10.5 kcal/mol on the most oxidized surface

TABLE 4: Normal-Mode Analysis for the TiC and VC Surface Complexes with CO[a]

surface	M−CO stretch (cm^{-1})	C−O stretch (cm^{-1})	k (M−CO) $m_M = 1000$	k (C−O) $m_M = 1000$	k (M−CO) m_M = at. wt.	k (C−O) mM = at. wt.
TiC (100)	320	2120	1.70	17.6	1.09	17.8
VC (100)	360	2060	2.25	15.9	1.47	16.1
ZnO (1010)	273	2202	1.01	19.21		
Cu (100)	260	2097	2.02	17.05		
Ni (100)	256	2069	3.98	15.87		

[a]Force constants are provided in units of mdyn/Å. The other values were adapted from D'Amico et al.[8]

studied.[28] Very limited π-back-bonding is expected for a fully oxidized Ti^{4+} species.

The first spectroscopic evidence for differences in π-back-bonding interactions on VC and TiC is the HREELS measured C−O stretching frequency for reversibly adsorbed CO on both surfaces. The 2060 cm^{-1} value on VC is similar to that observed on many metal systems where back-bonding occurs. Alternatively, the 2120 cm^{-1} frequency for CO reversibly adsorbed on TiC is only slightly lower than the gas phase. We acknowledge that other factors contribute to the measured C−O stretching frequency but the similarity of the substrate geometry, atomic masses, and chemical composition argue for enhanced π-bonding on VC. The HREELS data also indicate a CO species that is more weakly bound on VC than the predominant species found at lower coverages. This weakly adsorbed species is characterized by a V−CO stretching frequency of 230 cm^{-1} and higher C−O stretching frequency than the more strongly adsorbed species on VC. Although we cannot clearly assign this species, it may be a second phase of surface CO that corresponds to the low temperature shoulder observed in the TPD at higher coverages. We will address the existence of a strongly adsorbed CO species on TiC with a stretching frequency of 1990 cm^{-1} later in this discussion.

A normal-mode analysis was performed on the predominant reversibly adsorbed CO species on each surface using the XYZ-linear triatomic molecule as given in Herzberg.[30] The calculation was performed in two ways, first using the actual mass of the surface metal atom, and then by approximating the surface mass with a large number (1000 g) to restrict the surface motion. When our experimental values for the surface-CO and the C−O stretching frequencies are used, we obtain the force constants for the two bonds as presented in Table 4. We note that using the actual mass of the surface atom has little impact on the force constants for the C−O bond, but decreases the M−C value by approximately $^1/_3$. In comparing TiC to VC, we again see evidence for the stronger surface bond on VC by the greater calculated M−CO force constant. For either method of calculation, the M−CO bond force constant is 1.35 times greater on VC. In comparison to literature values, the Ti−CO force constant is greater than that calculated for ZnO (1.01 mdyn/Å for $m_{Zn} = 1000$), but clearly less than most metals. The value of the V−CO force constant is slightly larger than that for Cu (100), where the heat of adsorption is about −15 kcal/mol.[31]

The force constants calculated for the C−O bonds on the two carbide materials are both reduced from the gas-phase value (18.56 mdyn/Å).[47] We note that the force constant on VC has been reduced much more than on TiC, showing that the C−O bond has been weakened more on VC. These results are consistent with significantly more π-back-bonding on the VC surface, and in fact this force constant is comparable to that obtained from analyses of CO adsorbed to the Ni (100) surface.[32] The force constant on TiC is only slightly reduced from the gas phase value, and this small amount likely indicates that a very small amount of π-bonding is present. For example, results for Cu (100) generate a force constant of 17.05 mdyn/Å, where

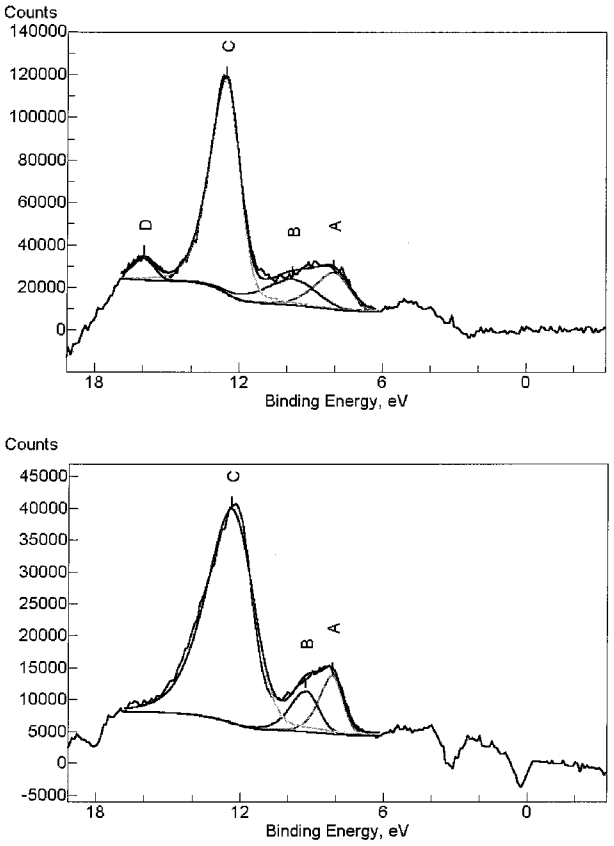

Figure 15. Fits to the UPS difference spectra for (a) CO/TiC and (b) CO/VC. In each fit, a Shirley background was used and the 4σ-1π (peaks C and B) energy splitting was fixed at 2.8 eV.

limited back-bonding is almost certainly present.[33] Alternatively, the lack of back-bonding on ZnO ($10\bar{1}0$) results in the force constant increasing above the gas-phase value.

The UPS data have great potential for direct insight into the nature of CO bonding on TiC and VC. The adsorption of CO to either surface should perturb valence levels of the adsorbate and the surface. Specifically, the σ-donor interaction of the CO 5σ orbital with unoccupied levels on the metal sites should perturb the 5σ significantly. On both TiC and VC, we do not clearly see the 5σ orbital in the UPS data as it has been stabilized by bonding interactions with the metal $3d_{z^2}$, 4s, and $4p_z$ orbitals, such that it overlaps with the 1π level, which is essentially nonbonding with respect to chemisorption. The greater splitting observed between the 4σ and the $1\pi/5\sigma$ UPS peaks on the TiC (4.3 eV) surface implies that the 5σ has been stabilized to a lesser extent on this surface than on VC (3.9 eV splitting). We note that this splitting is much greater than the $4\sigma-1\pi$ splitting in gas-phase CO, an effect that is due to the overlapping 1π and 5σ levels. When the data are fit with Gaussian peaks (peaks A−D on TiC and A−C on VC in Figure 15) and the $4\sigma-1\pi$ splitting is constrained at the gas-phase value of 2.8 eV, the $4\sigma-5\sigma$ splitting is 4.5 eV on TiC and 4.1 eV on VC, indicating

SCHEME 1

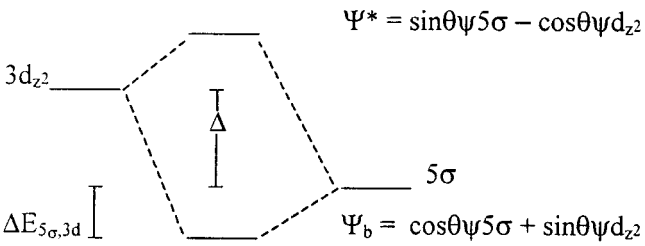

a 0.4 eV greater energy stabilization of the 5σ level on VC (Figure 15b).

The changes in the substrate valence features with adsorption are more subtle and somewhat masked by photoemission from other photon lines from the He resonance source. However, when the spectra are normalized to the intensities of the C 2p based features, we note very little difference between clean and CO adsorbed TiC. Alternatively, the VC 3d peak is clearly impacted by CO adsorption, losing intensity in the main UPS feature. The maximum of the peak shifts to deeper binding energy (by 0.1 eV) and a shoulder appears on the deeper binding energy side of the peak, shifted from the original intensity maximum by 0.4 eV. We assign this spectral change to an energy stabilization resulting from a measurable π-back-bonding interaction between the V 3d$_{xz,yz}$ orbitals and the CO 2π* level.

The valence photoemission data can be analyzed with a configuration interaction (CI) model developed by Van der Laan[36] and applied to CO adsorption by Solomon and co-workers.[7,37] This model uses photoemission data to quantify the energy stabilization brought about by chemical bonding. The 5σ orbital will be stabilized through bonding interactions with the empty metal 3d$_{z^2}$, 4s, and 4p$_z$. To simplify matters and to enable a comparison of the donor interaction between TiC and VC, we will consider only the 3d interaction but recognize that the total energy stabilization of the 5σ occurs from all three of these interactions. Scheme 1 shows the molecular orbitals involved in the bonding interaction, along with the relevant energy splittings and wave functions. The 5σ orbital is stabilized through the bonding interaction with an empty metal 3d by a value designated as $\Delta E_{5\sigma,3d}$. The energy separation of the two levels in the absence of bonding is designated Δ, and the resulting bonding (Ψ_b) and antibonding (Ψ*) orbitals are produced.

Neglecting overlap, the value of $\Delta E_{5\sigma,3d}$ is given by the following equation, where $H_{5\sigma,3d} = \langle\psi_{5\sigma}|H|\psi_{3d}\rangle$ is the bonding matrix element.

$$\Delta E_{5\sigma,3d} = \frac{\sqrt{[\Delta^2 + 4H_{5\sigma,3d}^2]} - \Delta}{2} \qquad (1)$$

The wave function coefficients are determined by the following relationship

$$\tan 2\theta = \frac{2\Delta H_{5\sigma,3d}}{\Delta} \qquad (2)$$

Suitable values for the values of $\Delta E_{5\sigma,3d}$ and Δ must be chosen to enable us to solve for $H_{5\sigma,3d}$ and θ. The value of ΔE will be taken as the change in the 4σ−5σ splitting in the UPS data compared to gas-phase CO, 1.2 eV for CO—TiC and 1.6 eV for CO—VC. We estimate a reasonable position for d$_{z^2}$ orbital of VC to be 1.0 eV above the Fermi level.[38] We assume that the 3d$_{z^2}$ position on TiC will be similarly split from its C 2p valence band feature, placing this level 1.6 eV above E_F. This generates values for Δ of 7.7 eV for CO—VC and 8.4 eV for CO—TiC. Inserting those values into eq 1, we calculate $H_{5\sigma,3d}$ values of 3.9 eV for VC and 3.4 eV for TiC, and θ values of 23 (VC) and 19 (TiC). The results indicate a slightly larger σ-contribution for CO adsorption on VC, but the results are quite similar.

A similar CI analysis can be made for the π-interaction. In this case, we must use the stabilization of the 3d level observed by the changes in the UPS spectrum of VC. Because there are no equivalent levels on TiC, we will assume that the π-contribution is virtually zero on TiC. For VC, we will use a value of 0.4 eV for the $\Delta E_{3d,2\pi^*}$. To determine a value of Δ, we must estimate the expected position of the 2π* level prior to bonding, which we place at 3.2 eV above E_F, based on a 4σ−2π* splitting of 15.6 eV.[39] This positioning gives a value of Δ = 3.7 eV, a $H_{3d,2\pi^*}$ of 1.3 eV, and θ = 17. Varying the value of Δ by ± 1 eV changes the value of $H_{3d,2\pi^*}$ by only 0.1 to 0.2 eV.[40] Assuming a negligible contribution from π-bonding on TiC, this means that the total σ and π-bonding interactions contribute 5.2 eV of energy stabilization for VC compared to 3.4 eV on TiC. If we assume similar repulsive interactions are present, then this implies that the bonding of CO to VC is approximately 1.5 times stronger. This result agrees reasonably well with our desorption enthalpies, the normal-mode analysis, and the DFT calculations.

The wave functions predicted by the values of θ give an estimate of the amount of covalent mixing of the levels involved. For TiC and VC, the respective wave functions for the 5σ-3d interaction become Ψ (TiC) = 0.95 $\psi_{5\sigma}$ + 0.33ψ_{3d} and Ψ (VC) = 0.92 $\psi_{5\sigma}$ + 0.39 ψ_{3d}. Therefore, the analysis predicts approximately 10% covalent mixing for TiC and 15% for VC for this interaction if the σ-bond were formed purely through 3d interactions. For the back-bonding interaction on VC, this analysis predicts approximately 9% mixing.

The only literature analyses that these results can be compared to are those done by Lin et al., for the CO/ZnO and CO/CuCl systems.[7] Both ZnO and CuCl, both materials have full d-bands and the σ-donor interaction of CO is believed to occur predominantly with the metal 4s. The analysis produced $H_{5\sigma,4s}$ values of 3.1 eV for ZnO and 4.8 eV for CuCl. Furthermore, the π-back-bonding energy for CuCl was determined to be 2.2 eV, whereas it was surmised that the π-bonding interactions with ZnO must be less than this, other spectroscopic evidence indicated no back-bonding. The interesting correlation to our work is in the heats of adsorption for CO on ZnO and CuCl, which are −12 kcal/mol and −23 kcal/mol respectively. In our results for TiC, very limited back-bonding has generated a 12 kcal/mol heat of desorption coupled to the 3.4 eV σ-bond energy, quite similar to ZnO.

The presence of satellites on both the C 1s and O 1s XPS peaks for CO adsorbed on both surfaces indicates that both systems have π-overlap and that adsorption is relatively weak on both surfaces, consistent with the desorption energies. Strongly adsorbed CO (typically on metals such as Ni where ΔH_{ads} = −28 kcal/mol) exhibits weaker satellites (I_{sat}/I_{main} = 0.35),[41] and satellites are not observed when back-bonding is absent due to a large energy separation between occupied d-levels and the 2π* level, such as on ZnO.[7] The origin of the satellites is a final state relaxation effect.[42] In essence, when a C 1s or O 1s core level is ionized on the CO molecule, the valence states involving the carbon or oxygen atoms are subjected to a greater effective nuclear charge, stabilizing these levels to deeper binding energy (see Scheme 2). Valence electrons involved in 2π* interactions can remain in different

SCHEME 2

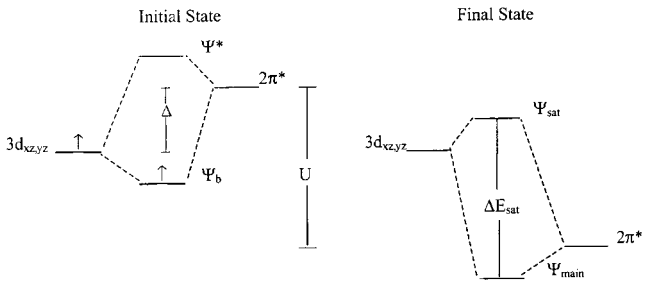

final states: either the electron remains in the relaxed $2\pi^*$ orbital that is predominantly located on the CO molecule, or it remains in the predominantly metal 3d based orbital that now lies at a much higher relative energy. In the data, the more stable final state is the main XPS peak, whereas the deeper binding energy satellite peak is the predominantly metal final state.

To have any intensity in the satellite, there must be some π-bonding interaction, that is some electron density must be present in a molecular orbital that has 3d-$2\pi^*$ overlap. In the initial state, this orbital (Ψ_b) will have predominantly metal (i.e., substrate) character. If the coupling between the surface and adsorbate is strong, there will be more $2\pi^*$ mixing into this molecular orbital. Upon ionization, therefore, the channel allowing relaxation into the more stable, relaxed $2\pi^*$ will be more likely, limiting satellite intensity. If the coupling is weak, then this channel becomes less likely and the metal based final state will have a greater population.

The core level satellite peaks can also be analyzed with the CI model. Referring to Scheme 2, the two possible final states are separated by ΔE_{sat}, which is defined by the following equation

$$\Delta E_{sat} = \sqrt{(U - \Delta)^2 + 4(H')^2} \tag{3}$$

As shown above, Δ is the initial state splitting between the unbonded 3d and $2\pi^*$ levels, U is the attraction between the final state core hole and the valence electrons (the relaxation of the valence levels), and H′ is the final state matrix element mixing the 3d and $2\pi^*$ levels in the presence of the core hole. As before, the wave function coefficients are defined by the relationship

$$\tan 2\theta' = \frac{2H'}{U - \Delta} \tag{4}$$

The resulting final state wave functions for the main peak and the satellite peak are

$$\Psi_{main} = \sin\theta'\psi_{3d} + \cos\theta'\psi_{2\pi^*}$$

$$\Psi_{sat} = \cos\theta'\psi_{3d} - \sin\theta'\psi_{2\pi^*}$$

The work of Van der Laan et al.[36] and Lin et al.[7] has generated a relationship for the relative intensity of the satellite to the main core level XPS peaks that depends only on the overlap of the wave functions. Given the wave functions written as above, this relationship should be as follows

$$\frac{I_{sat}}{I_{main}} = \left(\frac{\cos\theta'\cos\theta - \sin\theta'\sin\theta}{\sin\theta'\cos\theta + \cos\theta'\sin\theta}\right)^2 = \cot^2(\theta' + \theta) \tag{5}$$

This relationship is different from that developed by Van der Laan for cupric halides and used by Lin to describe CO adsorption where $I_{sat}/I_{main} = \tan^2(\theta' - \theta)$. However, the initial and final state wave functions used by Lin et al. and adapted here are different from the configurations used by Van der Laan to describe satellites in d^9 complexes, resulting in eq 5. In fact, eq 5 must be used to ensure that the final state wave functions are logical. Specifically for our work, we have values of I_{sat}/I_{main} for the VC C 1s level of 0.69, and $\theta = 17$ from our above analyses. These enable us to solve for θ', which we calculate to be 33. Importantly, the $\cot^2(\theta' + \theta)$ relationship predicts the experimental observation of greater satellite intensity with decreased π-bonding. As the sum of θ' and θ approaches zero, indicative of less 3d-$2\pi^*$ mixing in the final and initial states, the predicted satellite intensity increases. In the hypothetical case where a completely covalent bond exists in both initial and final states, $\theta = \theta' = 45°$, and the predicted satellite intensity goes to zero.

Returning to the CI model for the core level satellites, we can solve for the quantity $(U - \Delta) = (2H'/\tan 2\theta')$, substitute this into eq 3 and solve for H′ given our experimental values of $\Delta E_{sat} = 4.8$ eV and $\Delta = 3.7$ eV for VC. This calculation generates a value for H' of 2.2 eV, and $U = 5.7$ eV. We note that there is greater mixing and a greater interaction predicted for the final state wave functions than was predicted for the initial state. This is attributed primarily to the smaller value of $(U - \Delta)$ of 2.0 eV when compared to the $\Delta = 3.7$ eV in the ground state. As we do not have values of θ and Δ for the CO—TiC interaction, we cannot perform the same complete analysis. From eq 5, we can solve for the quantity $(\theta' + \theta) = 42$, somewhat less than the $(\theta' + \theta) = 50$ obtained for VC. All of these results are consistent with a weaker π-bonding interaction for CO on TiC in the ionized final state than observed for VC. The origin of π-bonding in the ground state for TiC is likely the presence of electron density in the $d_{xz,yz}$ orbitals present in the C 2p molecular orbitals arising from the strong covalent mixing between the metal and carbon atoms in these materials. Similar arguments have been recently made in discussions of the importance of π-bonding in CO adsorption on metals.[43] In that work, the CO 1π, $2\pi^*$ orbitals and metal d-orbitals of appropriate symmetry at varying energies due to band dispersion effects undergo configuration interaction to provide π-bond stability to the system. In contrast to our work, those studies of late transition metals argue for repulsive σ-interactions with full d-bands, which cannot be the case for materials having essentially empty d-orbitals and very weak π-bonding. Our results are more in keeping with the Blyholder model[44] with both materials capable of electron accepting σ-bonding interactions, and the dominant interaction creating π-bond stability between the empty CO $2\pi^*$ and an occupied 3d level on VC that is absent on TiC.

CO Decomposition. A small amount of CO decomposition was observed on both the VC and TiC (100) surfaces. The decomposition was characterized through the observance of three HREELS features that are not present for molecular CO adsorbed atop a single surface atom. These features were observed at 990, 1190, and 1405 cm^{-1} on TiC, and at 960, 1170, and 1385 cm^{-1} on VC. The very similar vibrational frequencies for both surfaces lead us to conclude that the same species are present on both materials. In addition, we observed a very stable 1990 cm^{-1} loss feature on TiC that retained intensity even at room temperature. We propose that this 1990 cm^{-1} feature is a CO molecule adsorbed to multiple titanium atoms on TiC (100), most likely at a carbon vacancy on the surface. C—O stretches in this range are usually attributed to adsorption at a 2-fold site.[45] Furthermore, the remaining surface spectral features share some similarities with those found after the adsorption and reaction

of O_2 and H_2O on VC (100), indicating some decomposition of CO. These features are minor ones in the H_2O surface chemistry, and we would expect other peaks, particularly the strong metal−hydrogen stretches, to be evident in this temperature range with water adsorption,[13] so we conclude that water contamination is unlikely. As with H_2O chemistry, the low concentrations of these species suggest that they are formed at defect sites and not on the terrace sites that dominate the CO desorption kinetics and spectroscopy on both TiC and VC.

As stated above, a likely defect site to initiate CO decomposition would be a carbon vacancy. Surface vacancies on TiC have been observed with scanning tunneling microscopy, although the chemical identity of the missing atom is unknown.[46] We feel carbon is the likely candidate as these materials have a tendency to be substoichiometric in carbon. Such a defect site would increase electron density on the metal atoms adjacent to the defect on either surface, enabling increased occupancy of the CO $2\pi^*$ level upon adsorption to promote decomposition.[29] The tendency for early transition metals such as Ti to decompose CO is well documented.[4] As presented in the results section, we attribute the 990 cm^{-1} peak on TiC and the 960 cm^{-1} peak on VC to the M═O species. The features at 1405 cm^{-1} (TiC) and 1385 cm^{-1} (VC) are ascribed to oxygen bound to both a carbon and a metal site in a three-centered bond in our previous work with water. The fairly high stretching frequency of this species implies that it must contain oxygen bonded to carbon, likely with some carbonyl character. The significant reduction from typical carbonyl frequencies is consistent with some interaction with a surface metal atom as well. In the present work, this species could be CO molecular adsorption in a different geometry or result from surface decomposition. The 1170 and 1190 cm^{-1} species are likely also bonded to multiple surface sites.

Very low C−O stretching frequencies have been reported on metal surfaces such as Fe (100),[20] Mo (110),[21] Cr (110),[48] and V (110).[49] In each case, the authors have concluded that the CO molecule is interacting with multiple surface sites, bonding both through the carbon atom and either the oxygen atom or π-orbitals. In particular, our results are strikingly similar to those observed on the Mo (110) surface, where a strong surface vibration was noted at 1345 cm^{-1}, and a weak loss feature at 1130 cm^{-1}. The authors concluded that these species were intermediates to decomposition to surface carbon and oxygen atoms. They surmised that the 1130 cm^{-1} form was Mo−C−O−Mo, the immediate precursor to dissociation, whereas the 1345 cm^{-1} feature was due to adsorbed CO interacting with two neighboring Mo atoms through its π-electrons. One can readily envision similar interactions at a carbon vacancy on the carbide surfaces, where four metal atoms in the surface layer are present to interact with the CO. The eventual production of the M═O species is consistent with the proposed decomposition precursors. The carbon atom from the CO molecule may fill the vacancy site in the lattice, although this is conjecture.

Comparison to DFT Results. As noted in the Results section, the energy stabilization calculated by DFT from the Ti_9C_9 cluster with CO bonded to the central Ti atom is very similar to our experimental desorption activation barrier, 12.7 vs 11.5 kcal/mol. The results for the V_9C_9 cluster indicate a much stronger interaction for CO with the VC surface, as an adsorption energy of −24.6 kcal/mol is predicted. This value is somewhat larger than we estimate from our experimental results (−18 kcal/mol), but the trend is clearly consistent with our experimental observation of a stronger VC−CO interaction. We also note that the repulsive interactions among CO molecules on the VC surface appear to be considerable and that our experimental estimate may be impacted by this and, hence, represent a lower estimate. We believe that the DFT calculations with the M_9C_9 clusters are providing reasonable estimates for the strength of the CO-surface interactions that could likely be improved upon with calculations using larger MC clusters

The other area of interest for comparison of our experiments and DFT calculations is in the measured energy positions of the valence features. In such a comparison, we recognize that the binding energies of the photoemission peaks are influenced by final state effects, and thus do not strictly adhere to Koopmans' theorem. Experimentally, we observe that the 5σ level is stabilized by 1.6 eV on VC and 1.2 eV on TiC, whereas the DFT results on the larger clusters predict 1.7 and 1.2 eV, respectively. As for the π-interactions, the DFT results predict very similar 0.5 to 0.6 eV destabilization for the $2\pi^*$ level upon adsorption to either TiC or VC. Experimentally, we observed a 0.4 eV shift of the d-levels on VC after CO adsorption. As the extent of π-overlap appears to be quite similar for the two materials, the key finding in this regard is that the metal orbitals involved in this interaction, the $3d_{xz,yz}$, are not occupied in TiC, but are in VC. This is precisely the prediction made by the MO diagram presented at the outset of this paper. Both the theory and the experiments, therefore, provide compelling evidence that a straightforward ligand field MO theory description of the bonding on the surfaces of these materials provides a qualitatively accurate picture of their electronic structure and bonding.

Conclusions

We have presented the first detailed spectroscopic examination of the interaction of CO with the TiC and VC (100) surfaces. This experimental work has shown conclusively that CO bonds more strongly with VC, primarily due to π-back-bonding interactions that are fundamentally absent on the TiC (100) surface. Such a result was predicted from a qualitative energy level diagram generated by MO theory and is supported by density functional calculations also performed in this work. On both materials, the presence of surface defects and the natural tendency to be substoichiometric generate reactive sites that have much different chemistry than the terrace atoms.

As a whole, these results and analyses show that the coordination chemistry of the terrace sites of the TiC (100) surface is essentially that of a d^0 species, that is the predominantly metal 3d-levels are unoccupied, precluding π-back-bonding (see Figure 1). The similar weak interaction of CO with TiO_2, where the titanium atom is clearly close to the formal d^0 oxidation state of +4, along with the spectroscopic results presented above argue for this remarkable result on TiC. However, it is clear from core level XPS data that the Ti atom in TiC does not exist in a true +4 oxidation state. Instead, the Ti core level binding energies are closer to the metal values, and our DFT results predict metal charges of approximately +0.8 for TiC and +1.1 for VC. The influence of the strong, directional carbon atom bonding interactions with the metal forces the metal valence electrons into bonding orbitals that are localized predominantly on the carbon atoms (Figure 1). However, the extent of the covalency between the metal (primarily through σ-bonding interactions) and the carbon must be dramatic to produce an effective metal charge of approximately +1, and this will be explored in future publications. Similarly, the coordination chemistry of the ideal VC (100) surface should be modeled as a d^1 species, with a single electron now occupying a predominantly metal d-orbital, leading to its

stronger π-bonding interaction with CO. Undoubtedly, the unique electronic environments of the carbides have the potential to be exploited in catalysis and in controlling the surface reactivity of these materials in tribological contacts.

Acknowledgment. The authors thank P. M. Adams of The Aerospace Corporation for his assistance with preparation of the crystal surfaces. This work was supported by the Independent Research and Development program at the Aerospace Corporation funded by the Space and Missile Systems Center of the United States Air Force Materiel Command, under Contract No. F04701-93-0094, and by the Air Force Office of Scientific Research under Contract Nos. F49620-97-0029 and F49620-00-1-0114.

References and Notes

(1) For example, see: Kawata, K. *Surf. Coat. Technol.* **1992**, *54/55*, 604. Boving, H. J.; Hintermann, H. E. *Tribol. Int.* **1990**, *23*, 129.

(2) (a) Lindberg, P. A. P.; Johansson, L. I. *Surf. Sci.* **1988**, *194*, 199. (b) Oshima, C.; Tanaka, T.; Aono, M.; Nishitani, R.; Kawai, S.; Yajima, F. *Appl. Phys. Lett.* **1979**, *35*, 822. (c) Oshima, C.; Aono, M.; Tanaka, T.; Kawai, S.; Zaima, S.; Shibata, Y. *Surf. Sci.* **1981**, *102*, 312. (d) Zaima, S.; Shibata, Y.; Adachi, H.; Oshima, C.; Potani, S.; Aono, M.; Ishizawa, Y. *Surf. Sci.* **1985**, *157*, 380. (e) Souda, R.; Aizawa, T.; Otani, S.; Ishizawa, Y.; Oshima, C. *Surf. Sci.* **1991**, *256*, 19. (f) Edamoto, K.; Anazawa, T.; Miyazaki, E.; Kato, H.; Otani, S. *Surf. Sci.* **1993**, *287/288*, 667. (g) Antonik, M. D.; Lad, R. J.; Christensen, T. M. *Surf. and Interface Anal.* **1996**, *24*, 681. (h) Ahn, J.; Kawanoowa, H.; Souda, R. *Surf. Sci.* **1999**, *429*, 338. (i) Oshima, C.; Aono, M.; Otani, S.; Ishizawa, Y. *Solid State. Commun.* **1983**, *48*, 911.

(3) For example, Fischer−Tropsch catalysis by TiC has been reported, see: Kojima, I.; Miyazaki, E.; Yasumori, I. *J. C. S. Chem. Commun.* **1980**, 573.

(4) Campuzano, J. C. in *The Chemical Physics of Solid Surfaces and Heterogeneous Catalysis*; King, D. A., Woodruff, D. P., Eds.; Vol. 3, p 389; Elsevier: Amsterdam, 1990.

(5) Föhlisch, A.; Nyberg, M.; Hasselström, J.; Karis, O.; Pettersson, L. G. M.; Nilsson, A. *Phys. Rev. Lett.* **2000**, *85*, 3309.

(6) Andersson, S. *Solid State Commun.* **1977**, *21*, 75.

(7) Lin, J.; Jones, P.; Guckert, J.; Solomon, E. I. *J. Am. Chem. Soc.* **1991**, *113*, 8312.

(8) D'Amico, K. L.; McFeely, F. R.; Solomon, E. I. *J. Am. Chem. Soc.* **1983**, *105*, 6380.

(9) Johansson, L. I. *Surf. Sci. Reports* **1995**, *21*, 177.

(10) Didziulis, S. V.; Lince, J. R.; Stewart, T. B.; Eklund, E. A. *Inorg. Chem.* **1994**, *33*, 1979.

(11) (a) Lowther, J. E.; Andiotis, A. *J. Phys. Chem. Solids* **1987**, *48*, 713. (b) Benco, L. *Solid State Commun.* **1995**, *94*, 861.

(12) Frantz, P.; Didziulis, S. V. *Surf. Sci.* **1998**, *412/413*, 384.

(13) Didziulis, S. V.; Frantz, P.; Perry, S. S.; El-bjeirami, O.; Imaduddin, I.; Merrill, P. B. *J. Phys. Chem. B* **1999**, *50*, 11129.

(14) Fischer, D. W. *J. Appl. Phys.* **1970**, *41*, 3561.

(15) Otani, S.; Honma, S.; Tanaka, T.; Ishizawa, Y. *J. Cryst. Growth* **1983**, *61*, 1.

(16) Olle, L.; Salmeron, M.; Baro, A. M. *J. Vacuum Sci. Technol. A* **1985**, *3*, 1866.

(17) Wu, M.-C.; Estrada, C. A.; Goodman, D. W. *Phys. Rev. Lett.* **1991**, *67*, 2910.

(18) Yates, J. T., Jr. *J. Vacuum Sci. Technol*. A **1987**, *5*, 1.

(19) Falconer, J. L.; Maddix, R. J. *Surf. Sci.* **1975**, *48*, 393.

(20) Benndorf, C.; Kruger, B.; Thieme, F. *Surf. Sci.* **1985**, *163*, L675.

(21) Chen, J. G.; Colaianni, M. L.; Weinberg, W. H.; Yates, J. T., Jr. *Chem. Phys. Lett.* **1990**, *177*, 113.

(22) Kuhlenbeck, H.; Saalfeld, H. B.; Buskotte, U.; Neumann, M.; Freund, H.-J.; Plummer, E. W. *Phys. Rev. B* **1989**, *39*, 3475.

(23) Sandell, A.; Bennich, P.; Nilsson, A.; Hernnäs, B.; Björneholm, O.; Mårtensson, N. *Surf. Sci.* **1994**, *310*, 16.

(24) Smith, R. J.; Anderson, J.; Lapeyre, G. J. *Phys. Rev. Lett.* **1976**, *37*, 108.

(25) For example, CO on Cu (111) displays a strong valence satellite, see: Freund, H. J.; Eberhardt, W.; Heskett, D.; Plummer, E. W. *Phys. Rev. Lett.* **1983**, *50*, 768.

(26) Gay, R. R.; Nodine, M. H.; Henrich, V. E.; Zeiger, H. J.; Solomon, E. I. *J. Am. Chem. Soc.* **1980**, *102*, 6752.

(27) Henrich, V. E.; Cox, P. A. *Applied Surf. Sci.* **1993**, *72*, 277.

(28) Raupp, G. B.; Dumesic, J. A. *J. Phys. Chem.* **1985**, *89*, 5240.

(29) Jensen, S. A.; Hoffmann, R. *Surf. Sci.* **1988**, *197*, 474.

(30) Herzberg, G. *Infrared and Raman Spectroscopy*; Van Nostrand Reinhold: New York, 1945, p 173.

(31) Cox, D. F.; Schulz, K. H. *Surf. Sci.* **1991**, *249*, 138.

(32) Sexton, B. A. *Chem. Phys. Lett.* **1979**, *63*, 451.

(33) Andersson, S. *Solid State Commun.* **1977**, *21*, 75.

(34) Van der Laan, G.; Westra, C.; Haas, C.; Sawatzky, G. A. *Phys. Rev B* **1981**, *23*, 4369.

(35) Solomon, E. I.; Jones, P. M.; May, J. A. *Chem. Rev.* **1993**, *93*, 2623.

(36) The DFT calculations performed in this work place the empty d_{z^2} orbital approximately 0.8 eV above the HOMO in the V_9C_9 cluster, and 12.7 eV above the C 2s levels. In the Ti_9C_9 cluster, the d_{z^2} is approximately 2 eV above the HOMO and 12.2 eV above the C 2s. For comparison, valence band XPS (free from the influence of the MVV Auger peak) place the C 2s at 11.8 eV on VC, and 10.9 eV on TiC, so locating the respective d_{z^2} levels at 1.0 and 1.6 eV above the Fermi levels is a reasonable approximation.

(37) In ref 7, the 4σ-$2\pi^*$ energy splitting is assumed to be approximately 15.9 eV in a similar analysis. As indicated earlier in this paper, our DFT calculation predicts a 4σ-$2\pi^*$ splitting of 14.9 eV in free CO.

(38) Because the UPS data do not clearly show the extent of d-level stabilization as a result of π-bonding, we also performed the analysis assuming that ΔE was 0.2 eV, producing a value of $H = 0.9$ eV, only slightly reduced from the value provided in the text.

(39) (a) Brundle, C. R.; Bagus, P. S.; Menzel, D.; Hermann, K. *Phys. Rev. B* **1981**, *24*, 7041. (b) Tillborg, H.; Nilsson, A,; Martensson, N. *J. Electron Spectrosc. Relat. Phenom.* **1993**, *62*, 73.

(40) (a) Bagus, P. S.; Seel, M. *Phys. Rev. B* **1981**, *23*, 2065. (b) Plummer, E. W.; Chen, C. T.; Ford, W. K.; Eberhardt, W.; Messmer, R. P.; Freund, H. J. *Surf. Sci.* **1985**, *158*, 58.

(41) Föhlisch, A.; Nyberg, M.; Bennich, P.; Triguero, L.; Hasselstrom, J.; Karis, O.; Pettersson, L. G. M.; Nilsson, A. *J. Chem. Phys.* **2000**, *112*, 1946.

(42) Blyholder, G. *J. Phys. Chem.* **1964**, *68*, 2772.

(43) (a) Sheppard, N.; Nguyen, T. T. in *Advances in Infrared and Raman Spectroscopy*; Clark, R. J. H., Hester, R., Eds.; Heyden: London, Vol. 5.1978. (b) Erley, W.; Ibach, H.; Lehwald, S.; Wagner, H. *Surf. Sci.* **1979**, *83*, 585.

(44) Frantz, P.; Didziulis, S. V.; Merrill, P. B.; Perry, S. S. *Tribology Letters* **1998**, *4*, 141.

(45) Bertel, E.; Stockbauer, R.; Madey, T. E. *Surf. Sci.* **1984**, *141*, 355.

(46) Chen, J. G.; Weisel, M. D.; Liu, Z.-M.; White, J. M. *J. Am. Chem. Soc.* **1993**, *115*, 8875.

(47) Hush, N. S.; Williams, M. L. *J. Mol. Spectrosc.* **1974**, *50*, 349.